Nanotechnology Perceptions
ISSN 1660-6795
www.nano-ntp.com

Influence of Er Substitution on Mg-Zn Nanoparticles' Magnetic Properties and Applications

***Ummed Singh[1], Ghewar Ram[2], Sahi Ram[3]**
[1, 2,3]*Mossbauer Laboratory, Department of Physics, Jai Narain Vyas University, Jodhpur, Rajasthan, India-342001*

Lanthanide Eribum substituted spinel ferrites with a composition of Zn0.6Mg0.4ErxFe2-xO4 (x=0.00,0.05,0.10 and 0.15) were synthesized by the co-precipitation method. X-ray diffraction studies relvealed the formation of single –phase cubic structure for all compositions. The lattice constant and crystallite size varied with increasing Er3+ content in Zn-Mg ferrite. 57Fe Mossbauer spectroscopic studied were carried out to determine the chemical state of iron, its occupaney and relarive amount in tetrahedral (A)site,octahedral(B) site or both .The obtain value of relative amount of iorn in the tetrahedral(A) site and octahedral(B) site or both was used to obtain the cation distribution at the tetrahedral (A) site and octahedral(B) sites. The cation distribution was used to determine the cation-cation distances and interionic bond angles to understand the spin interactions and the impact of Er3+ ion substitution on magnetic interactions in substituted Zn-Mg ferrites.
Keywords: Mossbauer spectroscopy, Zn-Mg ferrites, spinel ferrites, cation distribution.

1. Introduction

Ferrites are a class of magnetic materials that have attracted significant attention due to their unique magnetic properties and potential applications in various technological fields, such as magnetic recording, microwave devices, and magnetic sensors. Among the different types of ferrites, Zn-Mg ferrite has emerged as a promising material due to its high magnetic permeability, low coercivity, and excellent chemical stability. Doping Zn-Mg ferrite with rare earth elements, such as Erbium (Er), can further enhance its magnetic properties and tailor its magnetic behavior for specific applications.

The magnetic interactions in Er doped Zn-Mg ferrite play a crucial role in determining its magnetic properties, such as magnetic moment, magnetic anisotropy, and magnetic ordering. Understanding these magnetic interactions is essential for optimizing the magnetic properties of Er doped Zn-Mg ferrite and developing new magnetic materials with improved

performance. In this study, we investigate the magnetic interactions in Er doped Zn-Mg ferrite using Mossbauer spectroscopy , including magnetic measurements by VSM (Vibrating Sample Magnometer) and structural properties of all compositions by X-ray diffraction.

Many workers[1-5]have studied the $Zn_xMg_{1-x}Fe_2O_4$ composition (for $0 \leq x \leq 1.0$) and reported the changes in structural and magnetic properties with increase in Zn content.AllreportedZn-Mgferritecompositionsexhibitferromagnetic behavior. $Zn_{0.5}Mg_{0.5}Fe_2O_4$ has beenreported to have maximum magnetization value. $Zn_{0.5}Mg_{0.5}Fe_2O_4$ ferrite is a soft magnetic material and net magnetization contribution is due to the combined magnetic moments of magnetic sublattice-A and sublattice-B. Because the divalent ions Zn^{2+} and Mg^{2+} are diamagnetic in nature and have zero contribution to thenet magnetic moment, the magnetization of sublattice-A and sublattice-B in Zn-Mg ferrite will be due to the presence of Fe^{3+} magnetic ions. It is clear that in Zn-Mg ferrites,themagnetizationofsublattice-Aandsublattice-B will also change if there is a variation in the occupancy of Fe^{3+} ions in the tetrahedral and octahedral sites.

Several workers [6,7,8]have reported that when Fe^{3+} ions in ferrite are substituted by rare-earth ions, there is a substantial change in the structural and magnetic properties.Themagneticpropertiesareimproved owningto the increase in the magneto crystalline anisotropy, coercivity and saturation magnetization [9,10] The isotropic or anisotropic nature of the coercivity and saturation magnetization is in accordance to the variation in the contribution of the f-electron orbital to magnetic interaction [11] The anti ferromagnetic super exchange interaction between adjoining Fe^{3+} ions influences the magnetic properties of ferrites. When rare earth ions substitutes Fe^{3+} ions in spinel ferrite, RE^{3+}-Fe^{3+} interaction is induced, which modifies the intrinsic magnetic properties. In ferrites, because of larger distance between the cations, the exchange interaction arefavouredbyoxygenanionsandaretermedsuperexchange

interactions.Thesuperexchangeinteractionalsoplaysacrucialrole in the buildup of intrinsic magnetismin spinel structures. The interactions between cations via oxygen anions can be A-B and A-A or B-B interactions. In A-B interaction, all magnetic spins at the A-site are aligned in one direction and constitute magnetic sublattice-A while all magnetic spins at the B-site align in a directionopposite to the direction of the spins at the A-site andformmagnetic sublattice-B, resultinginnet magnetization in ferrite. The net magnetizationis givenbythe difference inthe magnetic momentsofsublattice-B and sublattice-A. The super-exchange interactions in ferrites are also affected by the distances and angles between the ion pairs inspinelstructure.LakhaniV.K.et.al.[12] and Kumar G. et. al, [13]reported that the magneticinteraction in substituted spinel ferrites is much more effective for certain angles and distances between the cation-cation and cation-anion ions. They showed that the distancesandanglesbetweenionpairsplayadecisiverole in spin interaction for certain favorable angles, and thatthe magnetic interaction is much more effective.

In present study, a series of Er^{3+} substituted $Zn_{0.6}Mg_{0.4}Er_xFe_{2-x}O_4$ (x=0.00, 0.05, 0.10 and

0.15) ferrites were synthesized and investigated by X-ray diffraction studies of their structural properties, VSM(Vibrating Sample Magnometer) studies for magnetic properties and ^{57}Fe Mössbauer spectroscopic studies to obtain the cation distribution in tetrahedral and octahedral sites and to estimate the magnetic interactions in Er^{3+} substituted $Zn_{0.6}Mg_{0.4}Fe_2O_4$ferrites.

2. Experimental

Materials and Methods

In the Co-precipitation method for synthesis ferrites, $Mg(NO_3)_26H_2O$, $Fe(NO_3)_39H_2O$, $Zn(NO_3)_26H_2O$, $Er(NO_3)_36H_2O$ were first dissolved in 300 mL of distilled water while preserving a 2:1 ratio. The precipitation procedure was started by adding a 1M NaOH solution drop wise while stirring continuously until the pH of the solution reached 10. The resultant precipitates were then washed by centrifuge with acetone and distilled water. The precipitates were then separated by filtering using a Buckner funnel. The precipitates were then dried in oven at 80°C for around 24 hours to remove any moisture. The sample was then ground and crushed from the dry residue to create a fine powder. This powder was calcined in order to finish the synthesis. The complete step by step procedure for synthesis of $Zn_{0.6}Mg_{0.4}Er_xFe_{(2-x)}O_4$(x=0.00,0.05,0.10 and 0.15) is pictorially represented in figure 1.

Mössbauer spectra were recorded at room temperature (300K) with a conventional constant acceleration spectrometer using a 10 mCi^{57}CO source embedded in Rhodiummatrix.Detailsoftheexperimentalset-uparesimilar as reported earlier by Nigam *et. al*.[14] Allspectra showing superposition of quadrupole doubletswere computer fitted to resolve them using a least square routine computer program written by Meerwall[15], assuming each spectrum to be a sum of Lorentzians functions. During the curve fitting, the width and intensity of the two halves of a quadrupole doublet wereconstrained to be equal. The quality of the fit was judged from the value of χ^2which was obtained close to 1.0 per degree of freedom in most of the cases. However, a deviation in the value of χ^2 has been accepted in some occasion when iterations did not improve the value of χ^2. The isomer shift (IS) value is reported with respect to the spectrum of standard iron foil of 25 μm thickness. Solid lines in the spectra reported here represent computer fitted curve and dots represent the experimental points.

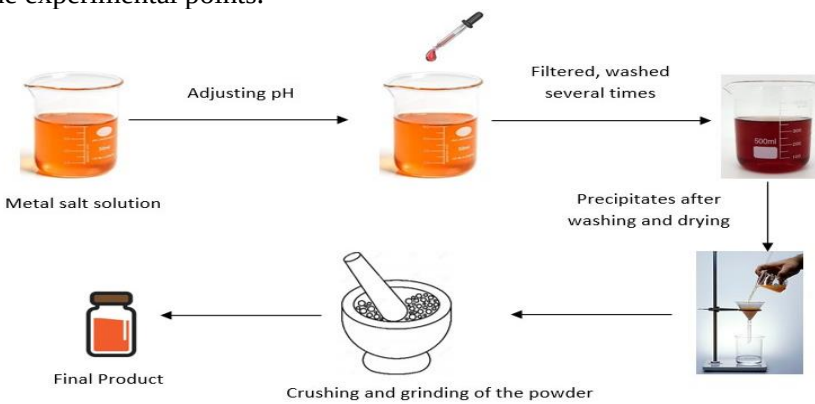

Figure -1 The complete step by step procedure for synthesis of $Zn_{0.6}Mg_{0.4}Er_xFe_{(2-}$

$_{x)}O_4$(x=0.00,0.05,0.10 and 0.15) is pictorially represented

3. Results and Discussion

Thex-raydiffractionpatternsobtainedfor Er^{3+} ions substituted Zn-Mg ferrite with compositions $Zn_{0.6}Mg_{0.4}Er_xFe_{2-x}O_4$(x=0.00,0.05,0.10 and 0.15)are displayed in Figure 1. The peaks indexed as (220), (311), (400), (422), (511) and (440) matches with (JCPDS card number73-1963 and ICDD# (00-034-0425.) From the high intense peak(311), the lattice constants (a) were calculated using following equation (1)[14] The Debye-Scherrer equation (2) was used to estimate the crystallite size 'D' of the samples, as detailed in equation table 2 [15].

$$a = d_{hkl}\sqrt{h^2 + k^2 + l^2} \quad (1)$$

Where *h,k,l,* are the index of diffraction peaks and $d_{hkl}$is the inter planner spacing.

Table 1: Calculation of Lattice Parameter (Å)obtained for $Zn_{0.6}Mg_{0.4}Er_xFe_{(2-x)}O_4$.(x=0.00, 0.05, 0.10 and 0.15)

Er Content (x)	θ	Sinθ	d_{hkl}	$\sqrt{h^2 + k^2 + l^2}$	Lattice Parameter (Å)
0.00	17.761	0.305047	2.525183	3.3166248	8.375086
0.05	17.668	0.303501	2.538048	3.3166248	8.417753
0.10	17.698	0.304	2.533883	3.3166248	8.40394
0.15	17.7235	0.303501	2.530354	3.3166248	8.392236

$$D = \frac{0.9\lambda}{\beta Cos\theta} \quad (2)$$

Where λ is wavelength of Cu-Kα radiation (1.5418Å)and β is full width at half maxima(FWHM) and θ is angle of diffraction at (311) are given in table 1.

Table 2: Calculation of crystalline size by Debye-Scherrer formula for $Zn_{0.6}Mg_{0.4}Er_xFe_{(2-x)}O_4$ (x=0.00, 0.05, 0.10 and 0.15)

Er Content (x)	θ	$Cos\theta$	β(FWHM)	D (nm)
0.00	17.761	0.952337	0.94847	0.59916
0.05	17.668	0.952831	0.78831	0.82037
0.10	17.698	0.952672	0.95142	0.82427
0.15	17.7235	0.952537	0.64371	0.82301

The presence of Er^{3+}cations As the dopant concentration of erbium increases, the lattice constant values also increase this behavior can be attributed to the differences in ionic radii between erbium and iron ions.Erbium has an ionic radius of 1.01 Å, whereas iron has an ionic radius of 0.645 Å. When erbium is introduced as a dopant in place of iron, it leads to an expansion of the lattice constant.However, when the erbium content exceeds x = 0.10, the lattice constant value starts to decrease. This shift in behavior can be explained by the limited solubility of erbium in comparison to iron, resulting from the larger ionic radius of Erbium.The XRD patterns also show a shift in peaks with changing dopent content, indicating variations in the lattice parameter.Another reason for the increase in the lattice

constant is the substitution of rare earth elements, as observed in comparison to pure copper nano ferrite samples. This increase can be attributed to the complete replacement of the smaller Fe^{3+} ions (0.645 Å) with the larger Er^{3+} ions (1.01 Å) in the copper ferrite structure, leading to an expansion of the lattice constant[17].

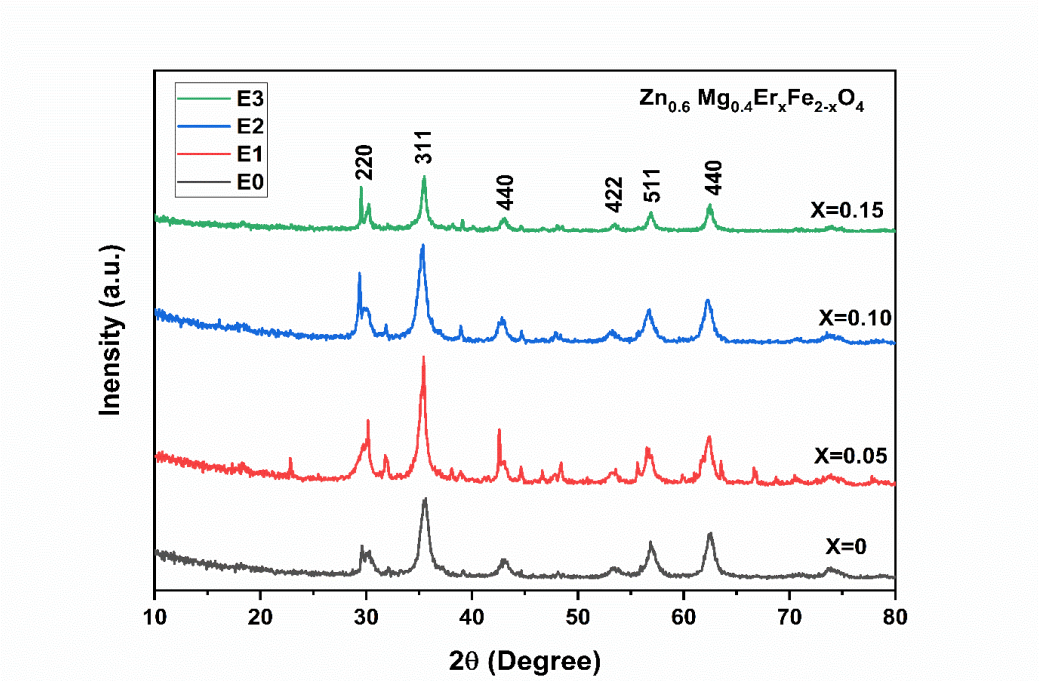

Figure2.X-raydiffractionpatternsobtainedinZn0.6Mg0.4ErxFe2-xO4(x=0.00, 0.05, 0.10 and 0.15)ferrites

Vibrating Sample Magnetometer (VSM):

Magnetization measurements were carried out using a vibrating sample magnetometer (VSM) at room temperature with a maximum applied magnetic field of 15 kOe. Figure-3shows the MH-loop of pure Er-doped $Zn_{0.6}Mg_{0.4}Er_xFe_{(2-x)}O_4$ (with x = 0.0, 0.05, 0.10 and 0.15)nanoparticles at room temperature.All the composite samples exhibit typical ferromagnetic hysteresis loops, indicating the presence of ordered magnetic structure. Magnetization of mixed spinel ferrites nanoparticles is strongly influenced by the cationic distribution on tetrahedral and octahedral lattice sites[18], [19]. The hysteresis curve (Figure 3) recorded at room temperature shows very low coercivity and remanence proves that the particles are superparamagnetic at room temperature. The saturation magnetization (M_s) value is 23.73emu/g for pure $ZnMgFe_2O$. The highest observed (M_s) value is 48.44 emu/g for x=0.15 and minimum of 19.88 emu/g for x=0.05. The saturation magnetization value increases with increasing the doping concentration of Erbiumin the $ZnMgFe_2O_4$. The increase in $M_s$indicated that the spontaneous magnetization in $Zn_{0.6}Mg_{0.4}Er_xFe_{(2-x)}O_4$ ceramic composites originates from the unbalanced antiparallel spins, which can give rise to the mentioned small coercivities[20]. The coercive field (H_c) for all the composite samples is larger than that for the pure $ZnMgFe_2O$.This increase is explained by the change in magnetic ion distribution in the spinelic network of Er ferrite where the Fe^{3+}ions are equally distributed in tetrahedral [A] and octahedral [B] positions, while the Zn^{2+} ions take

tetrahedral [A] site[21]–[22]. This leads to a decrease of magnetic moment in A-site. So the net magnetization increases, which is consistent with the increase of saturation magnetization[23].Therefore the magnetization of ZnMg-ferrite nanoparticles depends on the distribution of Fe3þ ions among tetrahedral and octahedral lattices sites because both Mg2þ and Zn2þ ions are non-magnetic in

nature. In nanoparticles, spins on the surface of nanoparticles also play an important role in determining magnetic properties[24]. It can affect the overall magnetic behavior of individual nanoparticles[25]. The decrease of magnetization with decreasing diameter of ferrite nanoparticles is a very well known effect, since the surface to volume ratio becomes of significant importance. The atoms on the surface have truncated bonds and less coordination neighbors, thus their mutual exchange interaction is reduced due to surface disorders. This surface disorder is due to bond frustration of exchange interaction between ferromagnetically coupled spins of different sublattices near the surface[26]. As the particle size gets smaller, such disorder and frustration at the nanoparticle's surface become progressively dominant due to large surface to volume ratio.

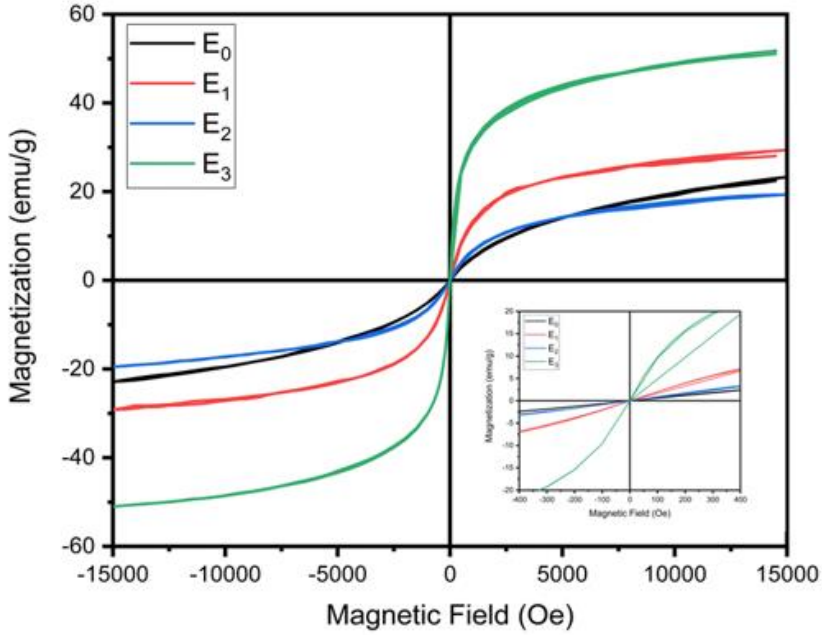

Figure-3 Magnetization hystresis loop at room tempreture for$Zn_{0.6}Mg_{0.4}Er_xFe_{2-x}O_4$(x=0.00, 0.05, 0.10 and 0.15)ferrites. The inset show the variation of magnetization at low applied field

The Mössbauer spectra of all synthesized samples recorded at room temperature are displayed in Figure 5. The concentration of Er^{3+} substitutions is mentioned inthe figure itself. The Mössbauer parameters obtained by the least square fitting of Lorentzians lines are given in Table 3.The isomer shift (IS) value is reported with respect to the spectrum of standard iron foil of 25μm thickness. In present study, the Isomer shift values are obtained ranging from 0.1 mm/s to 0.4 mm/s which attributes to iron in Fe^{3+} state [27,28] The

assignment of iron in Fe^{3+}state occupying either tetrahedral site or octahedral site is done in accordance with earlier reported work[29,30]The doublet with higher value of isomer shift is assigned to iron in Fe^{3+} state occupying the tetrahedralsite(A) whilethe doublet withsmallervalueof isomer shift is assigned to iron in Fe^{3+} state occupying the octahedral site (B).

From Table 4. it can be seen that in pure sample(x=0.00) the isomer shift value for site A is greater thanthatofsiteB.InasimilarstudyonZn-Mgferrites, WangJ.et.Al.[31] hasalsoreportedthistrendof larger isomer shift value ofsite-Aincomparisonto that of site-B.

Table3. Mossbauer parameters obtained in $Zn_{0.6}Mg_{0.4}Er_xFe_{2-x}O_4$(x=0.00, 0.05, 0.10 and 0.15)ferrites

ErCon tent(x)	Doublet		IS mms^{-1}	QS mms^{-1}	LW	RA
0.00	I	Fe^{3+} A-Site	0.36	0.48	0.53	84.55
	II	Fe^{3+} B-Site	0.34	0.83	0.49	15.45
0.05	I	Fe^{3+} A-Site	0.067	0.13	3.23	73.98
	II	Fe^{3+} B-Site	0.33	0.58	0.64	21.62
	I	Fe^{3+} A-Site	0.38	0.66	0.67	76.28
0.10	II	Fe^{3+} B-Site	0.35	0.26	0.75	23.72
0.15	I	Fe^{3+} A-Site	0.37	0.64	0.59	88.46
	II	Fe^{3+} B-Site	0.33	029	0.48	11.56

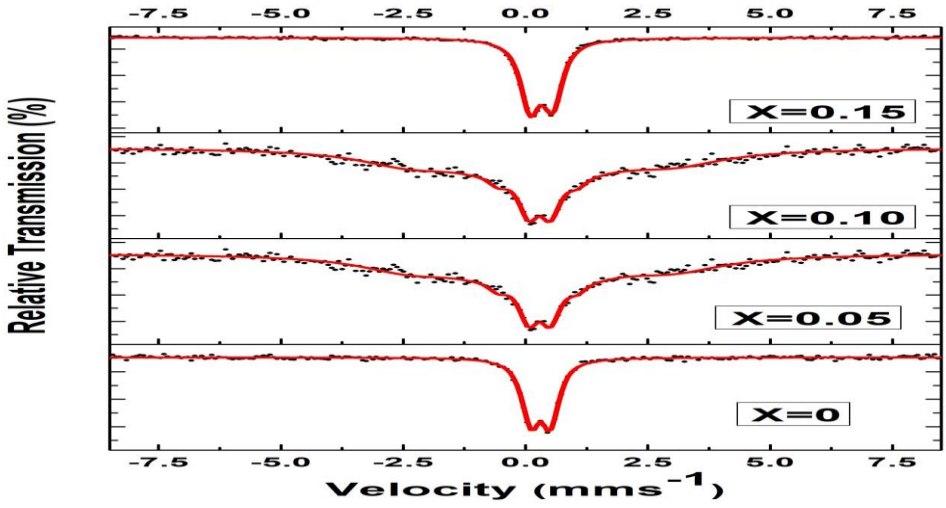

The amount of iorn in Fe^{3+} state occupying the tetrahedral site –(A) iorn Fe^{3+} state occupying octahedral site (B) can be estimated by the relative area of two quadruple doublets [32]. In pure sample (x=0.00) , the distribution of Fe^{3+} ions into A-site and B-site clearly indicate the formation of spinel Zn-Mg ferrite(x=0.00) is obvious due to the tendency of divalent ions Zn^{2+}having preferential occupancy to A-site while Mg $^{2+}$having preferential occupancy to B-site[33,34].

From Table 4.itcanalsobeseenthatforincreasing concentration of Er substitution, the relative amount of in tetrahedral site reduces while in octahedral site it increases. This clearly reflects the migration of Fe^{3+} ions towards octahedral site. It is obvious that the Fe^{3+} ions migrated from tetrahedral site to octahedral site will replace the Mg^{2+} ions from octahedral site because Er^{3+} ionsduetotheirlargerionic radii(0.88Å)haspreferential occupancy only to octahedral site.

In composition with x = 0.10, the Mössbauer spectrum exhibit only one central doublet corresponding to Fe^{3+} ion only in B-site. It reflects the complete migration of Fe^{3+} from tetrahedral site to octahedral site by replacing Mg^{2+} so that the tetrahedral site now has onlydivalent ions Zn^{2+} and Mg^{2+} while the octahedral site has only trivalent ions Fe^{3+} and Er^{3+} As earlier reported by Suwalkaet. al.[35] the cation distribution of tetrahedral site and octahedralsite in all compositions is estimated from Mössbauer spectra and is given in Table 5.

Table4. Estimated cation distribution in $Zn_{0.6}Mg_{0.4}Er_xFe_{2-x}O_4$ (x=0.00,0.05,0.10 and 0.15)

Er Content	A-site	B-sie
0.00	$Zn^{2+}_{0.6}\ Mg^{2+}_{0.31}\ Fe^{3+}_{0.09}$	$Mg^{2+}_{0.09}\ Fe^{3+}_{1.91}$
0.05	$Zn^{2+}_{0.432}\ Mg^{2+}_{0.4}\ Fe^{3+}_{0.168}$	$Zn^{2+}_{0.168}\ Er^{3+}_{0.5}\ Fe^{3+}_{1.782}$
0.10	$Zn^{2+}_{0.474}\ Mg^{2+}_{0.4}\ Fe^{3+}_{0.126}$	$Zn^{2+}_{0.126}\ Er^{3+}_{0.10}\ Fe^{3+}_{1.774}$
0.15	$Zn^{2+}_{0.6}\ Mg^{2+}_{0.230}\ Fe^{3+}_{0.170}$	$Mg^{2+}_{0.170}\ Er^{3+}_{0.15}\ Fe^{3+}_{1.68}$

Using the cation distribution given in Table 5. the average ionic radii at the tetrahedral site (r_A) and at octahedral sites (r_B) in all samples can be calculated by following relations [36]

$$r_A=\left[\left(C^A_{Zn^{2+}}\right)\left(r_{Zn^{2+}}\right)+\left(C^A_{Mn^{2+}}\right)\left(r_{Mg^{2+}}\right)+\left(C^A_{Dy^{3+}}\right)\left(r_{Dy^{3+}}\right)+\left(C^A_{Fe^{3+}}\right)\left(r_{Fe^{3+}}\right)\right]$$

$$r_B=\frac{1}{2}\left[\left(C^B_{Zn^{2+}}\right)\left(r_{Zn^{2+}}\right)+\left(C^B_{Mg^{2+}}\right)\left(r_{Mg^{2+}}\right)+\left(C^B_{Dy^{3+}}\right)\left(r_{Dy^{3+}}\right)\left(C^B_{Fe^{3+}}\right)\left(r_{Fe^{3+}}\right)\right]$$

Where $C^A$and C^B are the ionic concentration in A-sites and B-sites respectively, $r_{Zn}{}^{2+}$,$r_{Mg}{}^{2+}$,$r_{Er}{}^{3+}$and $r_{Fe}{}^{3+}$ are the radii of Zn^{2+},Mg^{2+},Er^{3+} and Fe^{3+} respectively

Table5.Lattice constant (a_{exp}), mean ionic radius of tetrahedral site (r_A) and octahedral site (r_B), theoretical value of Lattice constant (a_{th}) andoxygen positional parameter (u) in $Zn_{0.6}Mg_{0.4}Er_xFe_{2-x}O_4$(x=0,0.05,0.10and0.15)Ferrites

Er Content(x)	a_{exp} (Å)	r_A (Å)	r_B (Å)	a_{th} (Å)	u^{3m} 1/4,1/4,1/4	u^{43m} 3/8,3/8,3/8		
0.00	8.3750	0.7053	0.6313	8.3215	0.2205	0.3910	0.3905	0.3906
0.05	8.3917	0.6895	0.6455	8.3350	0.3218	0.3894	0.3891	0.3893
0.10	8.3909	0.6941	0.6494	8.3527	0.3181	0.3897	0.3892	0.3894
0.15	8.3922	0.7029	0.6513	8.3710	0.2810	0.3900	0.3895	0,3896

Using the values of radii of tetrahedral A-site (r_A) and mean radii of octahedral B-site (r_B), the theoretical values of lattice constant a_{th} for all samples can be obtained bythe relation [37]

$$a_{th}=\frac{8}{3\sqrt{3}}\left[(r_A+R_O)+\sqrt{3}(r_B+R_O)\right]$$

here $R_\circ$ is the radius of oxygen ion ($R_\circ$=1.32 Å)

ThecalculatedvaluesofmeanionicradiioftetrahedralA-site (r_A), mean ionic radii of octahedral B-site (r_B)and calculatedvalueoflatticeconstant'a_{th}'arelistedinTable5.ItisseenfromTable6thatinthesample(x=0)the mean ionic radii of tetrahedral site is more that the meanionic radii of tetrahedral site is more that the mean ionicradiiofoctahedralsite.Itisobviousbecausethe tetrahedral site is occupied by Zn^{2+} having ionic radius (0.74 Å) larger than the ionic radius (0.66 Å) which occupy octahedral site. When Er^{3+} ions are substituted with increasing concentration,the mean ionic radii of octahedral site increases but mean ionic radii of tetrahedral site show subtle change and remain almost unchanged.The increase in mean ionic radii is obviously duetothelargeionicradii (0.88Å)of Er^{3+}ions[38,39] The Er^{3+} ions have preferred occupancy to octahedral site because of larger interstices space in octahedral site . The Er^{3+} ions replaces Fe^{3+} ions in octahedral site , moreover from cation distribution given in Table 5, it is clear that the Fe^{3+} ions replaces Mg^{2+} ions from octahedral site and cause to migration of Mg^{2+} ions to tetrahedral site.. The ions involved in the compositions are having different ionic radii can cause a distortion in crystal symmetry. The distortion is also due to the internal stress by large ionic radii Er^{3+} ions enteringinto the octahedral site. Thelarge variation in theoretical value of lattice constant 'a_{th}' in comparisonto the experimentallycalculated value 'a_{exp}'is attributed to this distortion in crystal symmetry.

Furthermore, as the involved ions have different ionic radii, therefore to accommodate the incumbent ions in to either tetrahedral site or octahedral site, the oxygen anion may suffer a shifting from their actual position. So in spinel structure, the oxygen anion may or may not be present at their exact location in the FCC structure. The variation in position of oxygen anions is described in term of oxygen positional parameter 'u'.

The oxygen positional parameter u^{3m} value for center of symmetry at (1/4,1/4,1/4)

considering the origin at B-site is calculated by the relation [40]

$$u^{3m}=\frac{\frac{1}{4}R^2-\frac{2}{3}+\left(\frac{11}{48}R^2-\frac{1}{18}\right)^{1/2}}{2R^2-2}$$

Where $R=\frac{(B-O)}{(A-O)}$,the average bond length (B-O)= ($r_A+R_\circ$) and (A-O) = ($r_A+R_\circ$) are calculated using the mean ionic radii of A-site (r_A) and mean ionic radii of B-site (r_B) obtained from cation distribution .The $R_\circ$ corresponds to the ionic radii of oxygen anion (1.32 Å)

The oxygen positional parameter u^{43m} value for center of symmetry at (3/8,3/8,3/8) considering the origin at A-site is calculated by the relation [36]

$$u^{43m}=\frac{\frac{1}{2}R^2-\frac{11}{12}+\left(\frac{11}{48}R^2-\frac{1}{18}\right)^{1/2}}{2R^2-2}$$

$$u^{43m}=\frac{r_A+R_O}{a\sqrt{3}}+\frac{1}{4}$$

$$u^{43m}=0.3876\left(\frac{r_B}{r_A}\right)^{-0.07054}$$

From the table 6, it can be seen that the three values of $u^{43m}$of each individual composition are almost same inspite of being calculated by different formulas. For a FCCstructure,theidealvalueofu^{3m}fororiginatB-siteisu_{ideal}^{3m}=0.250Åandvalueof$u^{43m}$for origin at A-site is $u_{ideal}^{43m}=0.375$Å

Generally the ferrites show a deviation from this idealvalue of oxygen positional parameter 'u' and attain alarger value of 'u' in comparison to the ideal value [41,42] The deviation in 'u' value is also obtained in present study. From Table 6 it can be observed that when Er is substituted into Zn-Mg ferrite, the oxygen positional parameter value is slightly larger in value. However, for further increase in Er content, the value of 'u' further decreases. The decrease in value of 'u' indicates that the anions at B-site are moving away from cations at octahedral interstices due to the expansion of the octahedral interstices. The displacement of oxygen ions is in such a way that in A-B interaction the distancesbetween A and O ions are unchanged while the distance between B and O ions increases. Using the value ofoxygen positional parameter 'u' and experimental value of lattice constant 'a' for each composition, the bond lengths on tetrahedral site (d_{AX}), the bond length on octahedral site (d_{BX}), the length of tetrahedral shared edge (d_{AXE}), the length of octahedral shared edge (d_{BX}) and the unshared octahedral edge length (d_{BXEU}) are calculated by putting in the relations [43]

$$d_{AX}=a\sqrt{3}\left(u^{43m}-\frac{1}{4}\right)$$

$$d_{BX}=a\sqrt{\left[3(u^{43m})^2-\frac{11}{4}u^{43m}+\frac{43}{64}\right]}$$

$$d_{AXE}=a\sqrt{2}\left(2u^{43m}-\frac{1}{2}\right)$$

$$d_{BXE}=a\sqrt{2}(1-2u^{43m})$$

$d_{BXEU}=a\sqrt{\left[4(u^{43m})^2-3u^{43m}+\frac{11}{16}\right]}$

The calculated values of bond lengths, shared edge lengths and unshared octahedral edge length are listed in Table 6. The variations of d_{AX} and d_{BX} with increasing Er contentisdisplayedinFigure6(a)andthevariationofd_{AXE}, d_{BXE}, and d_{BXEU} with increasing content of Er are displayed in Figure 6(b).

Table6. Bond length at tetrahedral site(d_{AX}), bond length at octahedral site(d_{BX}) , shared tetrahedral edge length (d_{AXE}) , shared octahedral edge length (d_{BXE}) and unshared octahedral edge length (d_{BXEU}) in $Zn_{0.6}Mg_{0.4}Er_xFe_{2-x}O_4$ (x=0.00,0.05,0.10 and 0.15)

Er Content (x)	d_{AX} (Å)	d_{BX} (Å)	d_{AXE} (Å)	d_{BXE} (Å)	d_{BXEU} (Å)
0.00	2.0250	1.9604	3.3205	2.6055	2.9542
0.05	2.0124	1.9688	3.2858	2.6069	2.9551
0.10	2.0215	1.9750	3.2880	2.6065	2.9527
0.15	2.0385	1.9739	3.3143	2.6041	2.9682

Withthesubstitutionof Er^{3+}ioncontent,thebondlength andedgelengthontetrahedral sitedoesnotchangebutthe bond length and edge length on octahedral site increases. Theunsharededgelengthonoctahedralsitealsoremain unchangedbutslightlyincreasesathigherconcentration of Er^{3+}ionssubstitution (x=0.10and0.15).Thisobservedtrend of bond lengths and edge lengths is in conformity with the observed ionic radii of tetrahedral site and octahedral site indicating the expansion in octahedral site.

The inter-ionic distances the cation-cation(M_e-M_e) (b,c, d,e,and f) and between cation-anion(M_e-O) (p, q, r and s) has been calculated using the experimental value of lattice constamt (a_{exp}) and oxygen positional parameter (u^{3m}) in the following relation [43]

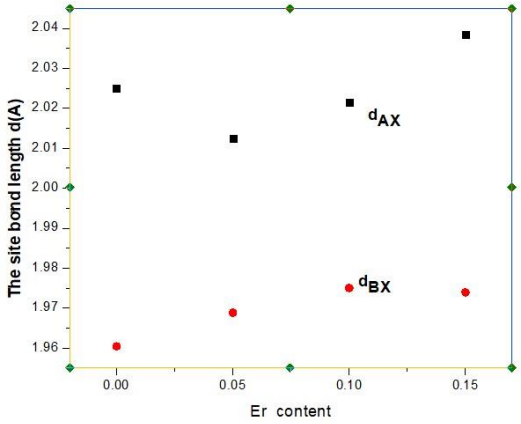

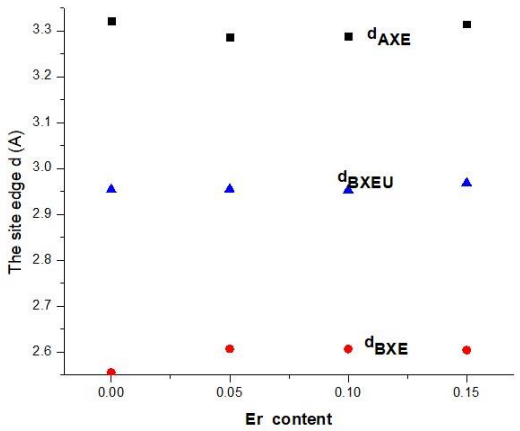

Figure4. Variations of A-site bond length and B-site edge with Er^{3+} content

$$M_e - M_e$$

$$b = \left(\frac{a}{4}\right)\sqrt{2}$$

$$c = \left(\frac{a}{8}\right)\sqrt{11}$$

$$d = \left(\frac{a}{4}\right)\sqrt{3}$$

$$e = \left(\frac{3a}{8}\right)\sqrt{3}$$

$$f = \left(\frac{a}{4}\right)\sqrt{6}$$

$$M_e - O$$

$$p = a\left(\frac{1}{2} - u^{3m}\right)$$

$$q = a\left(u^{3m} - \frac{1}{8}\right)\sqrt{3}$$

$$r = a\left(u^{3m} - \frac{1}{8}\right)\sqrt{11}$$

$$s = \frac{a}{3}\left(u^{3m} + \frac{1}{2}\right)\sqrt{3}$$

Using the values of inter-ionic distance betweencation-cation and cation-anion, the bond angles are calculated by following relations [12]

$$\theta_1 = \cos^{-1}\left[\frac{p^2 + q^2 - c^2}{2pq}\right]$$

$$\theta_2 = \cos^{-1}\left[\frac{p^2 + r^2 - e^2}{2pr}\right]$$

$$\theta_3 = \cos^{-1}\left[\frac{2p^2 - b^2}{2p^2}\right]$$

$$\theta_4 = \cos^{-1}\left[\frac{p^2 + s^2 - f^2}{2ps}\right]$$

$$\theta_5 = \cos^{-1}\left[\frac{r^2 + q^2 - d^2}{2rq}\right]$$

The calculated values of inter-ionic distances between cation-cation, cation-anion and bond angles are listed in Table 7. It is noted that with increasing Er content the inter-ionicdistancebetweencation-cationandcation-anion distance also increases slowly (except q and r). Since the inter-ionic distances are related to the lattice constant, the small increase in inter-ionic distance with Er content (x)is in agreement with small increase in lattice constant 'a_{exp}'. In composition with larger Er content (x=0.15), the bond length and shared edge length of tetrahedral site is slightly increases. This distinct pattern is attributed tolarge sized Er^{3+} ions accumulated at the boundary and cause partial stretching of tetrahedral site away from octahedral site

Table 7.cation-cation distances (b, c, d, e, f), cation-anion distances(p, q, r, s) and inter-ionic bond angles obtained in $Zn_{0.6}Mg_{0.4}Er_xFe_{2-x}O_4$(x = 0.00, 0.05, 0.10 and 0.15) ferrite

Cation-Cationdistances (M_e-M_e)	Er Content (x)			
	0.00	0.05	0.10	0.15
b(Å)	2.9605	2.9664	2.9661	2.9666
c(Å)	3.47209	3.4790	3.4786	3.4792
d(Å)	3.62637	3.6336	3.6332	3.6338
e(Å)	5.43956	5.4504	5.44498	5.4507
f (Å)	5.12861	5.1388	5.1383	5.1391
Cation-Aniondistances (M_e-O)				
p(Å)	2.3408	1.4954	1.5271	1.8374
q(Å)	1.3857	2.8603	2.8073	2.2682
r (Å)	2.6534	5.4773	5.3757	4.3434
s (Å)	3.4838	3.9814	3.9621	3.78426
Inter-ionicangles(degree)				
θ_1	44.14	78.63	102.718	115.467
θ_2	68.02	81.12	84.65	117.90
θ_3	78.45	165.35	152.409	107.636
θ_4	57.86	134.32	72.86	128,80
θ_5	55.27	37.135	38.628	56.7428

The bond angles θ_1, θ_2 and θ_5 corresponds to super exchange A-B and A-A interaction while

the bond angleθ_3 and θ_4 corresponds to B-B interactions. The strength of interactions is directly proportional to the bond angle and inverselyproportionaltothebondlength. From Table 7 and Figure 6, it is noted that with increasing Er^{3+} content the bond length and shared edge length at octahedral site increases. This increase in bond length weakens the A-B interaction despite the increase in bond angles.

4. Application

The capability of the nanoconstruct to accumulate at intracellular level granted by its high targeting efficacy toward melanoma cells causes a satisfactory reduction of cell viability in spite of the low temperature increase produced by the magnetic seeds, as observed in the calorimetric measurements. However, for the size range imposed by the protein shell of ferritins, the Co doping appears as a mandatory requirement in order to deliver the minimal amount of energy to make the apoptotic process efficient. Importantly, Co-doped HFt-MSH-NPs represents an example of an extremely small functionalized targeting nanosystem exploitable for MFH. Both the use of a targeted physiological protein and the reduction of the total size of therapeutic carrier are of paramount importance for in vivo applications, allowing for a selective cellular uptake, meanwhile reducing the risk of associated side effects. Finally, our result suggests that a different approach, which tries to take into account the system as a whole rather than focusingon a single physical functionality, should be pursued to realize efficient antitumoral agents. Moreover, the possibility of further functionalizing the nanoconstruct with chemotherapeutic agents may open the way toward a multimodal approach in which NP-mediated heat release can amplify the cytotoxic drug action.superparamagnetic hyperthermia (SPMHT), the very high magnetic anisotropy of $CoFe_3O_4$ ferrite nanoparticles compared to that of F_3O_4 magnetite, radically influences the hyperthermia effect, which is reflected in the specific loss power and, finally, on the heating temperature of the nanoparticles [42,43]. As a result, the maximum effect in SPMHT given by the specific loss power is obtained in the case of soft nanoparticles of Fe_3O_4 for a diameter (size) of nanoparticles (approximately spherical) of ~16 nm, and in the case of $CoFe_2O_4$ hard ferrite nanoparticles for a diameter of only ~6 nm (the exact value depending on the frequency of the alternating magnetic field). In terms of SPMHT which uses superparamagnetic nanoparticles, these nanoparticle sizes would be too large for Fe3O4 nanoparticles and too small for $CoFe_2O_4$ nanoparticles, both types of nanoparticles thus having advantages and disadvantages in magnetic hyperthermia for cancer therapy. More detailed results and discussions were presented on these issues [42,43].

5. Conclusion

The substitution of Er^{3+} ions in Zn-Mg ferrite done by co-precipitation method resulted into the synthesis of $Zn_{0.6}Mg_{0.4}Er_xFe_{2-x}O_4$(x = 0.00, 0.05, 0.10 and 0.15) ferrites. Withthe substitutionoflarger ionic radii Er^{3+}ioninto B- site of Zn-Mg ferrite, the structural properties are found tochange with increase in Ercontent. The substitution of Er^{3+} ions in Zn-Mg ferrite has also changed the cation distribution of tetrahedral site and octahedral site. The cation distribution changes drastically with increase in Er content. Furthermore, with the inclusion of Er^{3+} ion in increasing concentration, the variation of bond angles indicates the strengthening of super exchange interaction but the increase in bond length of octahedral site and the increasing trend of cation-cation inter-ionic distances

contradicts. It is inferred that in Er^{3+} substituted Zn-Mg ferrites, magnetic properties are expected to improve. In compositions with large concentration of Er substitution,a hindrance to magnetic properties is also expected. The magnetic interactions in Er-substituted Zn-Mg ferrite indicate change in microscopic magnetic properties.

References

1. Manikandan, A., Judith Vijaya, J., Sundararajan, M.,Meghanathan,C.,JohnKennedy,L.andBuoudina,M.,"Optical and magnetic properties of Mg-doped $ZnFe_2O_4$nanoparticlespreparedbyrapidmicrowavecombustionmethod",SuperLatt.AndMicro str.,Vol.64,pp.118-131(2013).
2. Rodriguez-Reyes,P.Y.,Hernandez-Cortes,D.A.,Escobedo-Bocardo,J. C.,Almanza-Robles, J. M., Sanchez-Fuentes,H.J.,Jasso-Teran, A., De-Leon-Prado, L. E., Mendez-Nonell, J. andHurTado-Lopez,G.F.," Structural and magnetic propertiesofMg-Znferrites($Mg_{1-x}Zn_xFe_2O_4$)preparedbysol-gelmethod",
3. J.Magn.Magn.Mater.,Vol.427,pp.268-271(2017).
4. Choodamani, C., Rudraswamy, B. and Chandrappa, G.T.,"Structural, electrical, and magnetic properties of znsubstitutedmagnesium ferrite", Ceram. Int., Vol. 42(9), pp. 10565-10571(2016).
5. Goya, G. F. and Rechenberg, H. R., "Ionic disorder and Néeltemperature in $ZnFe_2O_4$nanoparticles" J. Magn. Magn. Mater.,Vol. 196-197, pp. 191-192 (1999).
6. Masina, P., Moyo, T. and Abdallah, H. M. I., "Synthesis,structuralandmagneticpropertiesof$Zn_xMg_{1-x}Fe_2O_4$nanoferrites",J.Magn.Magn.Mater.,Vol.381,pp.41-49(2015).
7. Phor, L., and Kumar, V., "Structural, magnetic and dielectricpropertiesoflanthanumsubstituted$Mn_{0.5}Zn_{0.5}Fe_2O_4$",Ceram.Int., Vol. 45, pp. 22972-22980 (2019).
8. Pachpinde,A.M.,Langade,M.M.,Lohar,K.S.,Patange,S.M.andSagar, E. S, "Impact of larger rare earth Pr^{3+}ions on the physicalproperties of chemically derived $Pr_xCoFe_{2-x}O_4$nanoparticles",Chemical physics", Vol. 429, pp. 20-26 (2014)
9. Rezlescu,N.,Rezlescu,E.,Pasnicu,C.andCraus,M.L.,"Effectsoftherare-earthionsonsomepropertiesofanickel-zinc ferrite", J. Phys: Condens Matter., Vol. 6, pp. 5707-5716(1994).
10. Biao, Z., Ya-Wen, Z., Chun-Sheng, L/, Chun-Hua, Y., Liang-Yao,C.andSong-You,W.,"Rare-earth-mediatedmagnetismand magneto-optical Kerr effects in nanocrystalline$CoFeMn_{0.9}RE_{0.1}O_4$thin films", J. Magn. Magn. Mater., Vol.280(2-3), pp. 327-333 (2004).
11. Peng, J., Hojamberdiev, M., Xu, Y.,Cao,B.,Wang, J.andWu,H.,"Hydrothermal synthesis and magnetic properties of gadolinium-doped $CoFe_2O_4$nanoparticles", J. Magn. Magn. Mater., Vol.323(1), pp. 133-137 (2011).
12. Akamatsu, H., Kawabata, J., Fujita, K., Murai, S. and Tanaka, K.,"Magnetic properties of oxide glasses containing iron and rareearth ions", Phys. Rev. B 84, 144408 (2011).
13. Lakhani,V.K.,Pathak,T.K.,Vasoya,N.H.andModi,K.B.," Structural parameters snd x-ray Debye temperaturedetermination study on copper-ferrite-aluminates", Solid StateSci., Vol. 13, pp. 539-547 (2011
14. Biao, Z., Ya-Wen, Z., Chun-Sheng, L/, Chun-Hua, Y., Liang-Yao,C.andSong-You,W.,"Rare-earth-mediatedmagnetismand magneto-optical Kerr effects in nanocrystalline$CoFeMn_{0.9}RE_{0.1}O_4$thin films", J. Magn. Magn. Mater., Vol.280(2-3), pp.

327-333 (2004).
15. Peng, J., Hojamberdiev, M., Xu, Y.,Cao,B.,Wang, J.andWu,H.,"Hydrothermal synthesis and magnetic properties of gadolinium-doped CoFe2O4nanoparticles", J. Magn. Magn. Mater., Vol.323(1), pp. 133-137 (2011).
16. Akamatsu, H., Kawabata, J., Fujita, K., Murai, S. and Tanaka, K.,"Magnetic properties of oxide glasses containing iron and rareearth ions", Phys. Rev. B 84, 144408 (2011).
17. Peng, J., Hojamberdiev, M., Xu, Y.,Cao,B.,Wang, J.andWu,H.,"Hydrothermal synthesis and magnetic properties of gadolinium-doped CoFe2O4nanoparticles", J. Magn. Magn. Mater., Vol.323(1), pp. 133-137 (2011).
18. Yu X, Yang R, Wu C, et al (2023) Effect of Cr3+ Doping on Magnetic Properties of Zn-Mg Ferrite Nanoparticles. Magnetochemistry 9:181. https://doi.org/10.3390/magnetochemistry9070181
19. Komal, Kumar A, Kumar Y, Shukla VK (2023) Partheniumhysterophorus derived activated carbon for EDLC device application. J Mater Sci: Mater Electron 34:1880. https://doi.org/10.1007/s10854-023-11309-6
20. Mustaqeem M, Mahmood K, Saleh TA, et al (2020) Synthesis of CuFe2–xErxO4 nanoparticles and their magnetic, structural and dielectric properties. Physica B: Condensed Matter 588:412176. https://doi.org/10.1016/j.physb.2020.412176
21. Md. M. Roni, K. Hoque, T. C. Paul, M. N. I. Khan, and Md. E. Hossain, "Synthesis of La-doped Mn0·6Zn0.4LaxFe2-xO4 and the study of its structural, electrical and magnetic properties for high frequency applications," *Results Mater.*, vol. 11, p. 100215, Sep. 2021, doi: 10.1016/j.rinma.2021.100215.
22. D. H. Manh, T. D. Thanh, T. L. Phan, and D. S. Yang, "Towards hard-magnetic behavior of CoFe2O4 nanoparticles: a detailed study of crystalline and electronic structures, and magnetic properties," *RSC Adv.*, vol. 13, no. 12, pp. 8163–8172, Mar. 2023, doi: 10.1039/D3RA00525A.
23. J. S. Malhotra, A. K. Singh, R. Khosla, S. K. Sharma, G. Sharma, and S. Kumar, "Investigations on structural, optical and magnetic properties of Fe and Dy co-doped ZnO nanoparticles," *J. Mater. Sci. Mater. Electron.*, vol. 29, no. 5, pp. 3850–3855, Mar. 2018, doi: 10.1007/s10854-017-8321-4.
24. K. Ashok Kumar, A. Pandurangan, S. Arumugam, and M. Sathiskumar, "Effect of Bi-functional Hierarchical Flower-like CoS Nanostructure on its Interfacial Charge Transport Kinetics, Magnetic and Electrochemical Behaviors for Supercapacitor and DSSC Applications," *Sci. Rep.*, vol. 9, no. 1, Art. no. 1, Feb. 2019, doi: 10.1038/s41598-018-37463-0.
25. J. Ma *et al.*, "High-entropy spinel ferrites MFe2O4 (M = Mg, Mn, Fe, Co, Ni, Cu, Zn) with tunable electromagnetic properties and strong microwave absorption," *J. Adv. Ceram.*, vol. 11, no. 5, pp. 754–768, May 2022, doi: 10.1007/s40145-022-0569-3.
26. T. N. Pham, T. Q. Huy, and A.-T. Le, "Spinel ferrite (AFe2O4)-based heterostructured designs for lithium-ion battery, environmental monitoring, and biomedical applications," *RSC Adv.*, vol. 10, no. 52, pp. 31622–31661, Aug. 2020, doi: 10.1039/D0RA05133K.
27. B. Thakur, Y. Kumar, M. Gupta, U. P. Deshpande, N. V. Chandra Shekar, and S. Chakravarty, "Investigating the effect of thickness on the structural and magnetic properties of carbon thin film," *Carbon*, vol. 191, pp. 205–214, May 2022, doi: 10.1016/j.carbon.2022.01.060.
28. R. Javed, M. Zia, S. Naz, S. O. Aisida, N. ul Ain, and Q. Ao, "Role of capping agents in the application of nanoparticles in biomedicine and environmental remediation: recent trends and future prospects," *J. Nanobiotechnology*, vol. 18, no. 1, Art. no. 1, Dec. 2020, doi: 10.1186/s12951-020-00704-4.
29. B. Issa, I. M. Obaidat, B. A. Albiss, and Y. Haik, "Magnetic Nanoparticles: Surface Effects and Properties Related to Biomedicine Applications," *Int. J. Mol. Sci.*, vol. 14, no. 11, Art. no. 11, Nov. 2013, doi: 10.3390/ijms141121266.

30. K. Nadeem, H. Krenn, T. Traussnig, R. Würschum, D. V. Szabó, and I. Letofsky-Papst, "Effect of dipolar and exchange interactions on magnetic blocking of maghemite nanoparticles," *J. Magn. Magn. Mater.*, vol. 323, no. 15, pp. 1998–2004, Aug. 2011, doi: 10.1016/j.jmmm.2011.02.041.
31. Kumar,S.,Farea,A.M.M.,Batoo,K.M.,Lee,C.G.,Koo,B.H.andYonsef, A., "Mössbauer studies of $Co_{0.5}Cd_xFe_{2.5-x}O_4 (0.0 \leq x \leq 0.5)$ ferrite",PhysicaB:Condensedmatter,Vol.403(19-20),pp.3604-3607 (2008).
32. Eltabey, M.M., Massoud, A.M. and Radu, C., "Microstructure andSuperparamagnetic Properties of Mg-Ni-CdFerritesNanoparticles", Journal of nanomaterials, Vol. 204, pp. 492832(2014).
33. Wang, J., Zeng, C., Peng, Z. and Chen, Q., "Synthesis andmagnetic properties of $Zn_{1-x}Mn_xFe_2O_4$nanoparticles" Physica B"Vol. 349 (1-4), pp. 124-128 (2004).
34. Gupta, M. and Randhawa, B.S., "Mössbauer, magnetic andelectric studies on mixed Rb–Zn ferrites prepared by solutioncombustion method", Mat. Chem. and phys., Vol. 130, pp. 513-518 (2011
35. Suwalka, O., Sharma, R. K., Sebastian, V., Laxm,i N. andVenogopalan, K., "A study of nanosized Ni substituted Co-Znferrite prepared by coprecipitation", J. Magn. Magn. Mater., Vol.313, 198-203 (2007).
36. Mohammed, K.A., Al-Rawas, A.D., Gismelseed, A.M., Setlai, A.,Widatallah, H.M., Yousif, A., Elzain, M.E. and Shongwe, M.,"Infraredandstructuralstudiesof$Mg_{1-x}Zn_xFe_2O_4$ferrites",PhysicaB, Vol. 407, pp. 795-804 (2012).
37. Phor, L., Chahal, S. and Kumar, V., "Zn^{2+} substitutedsuperparamagnetic$MgFe_2O_4$spinel-ferrites: Investigation onstructuralandspin-interactions",J.Adv.Ceram.,Vol.9(5),
38. pp.576-587(2020).
39. Globus, A., Pascard, H. and Cagan, V., "Distance betweenmagnetic ions and fundamental properties in ferrite" Journal ofPhys. Colloques, Vol. 38, pp. 163-168 (1977).
40. Mazen, S.A., Abdallah, M.H., Sabrah, B.A., and Hashem, H. A.M., "The Effect of Titanium on Some Physical Properties of$CuFe_2O_4$" Physica Status solidi (a), Vol. 134(1), pp. 263-271(1992).
41. Chouhan, B. S., Kumar, R., Jadhav, K. M. and Singh, M.,"Magnetic study of substituted Mg-Mn ferrites synthesized bycitrate precursor method" J. Magn. Magn. Mater., Vol. 283, p 71(2005).
42. Kumar, G., Kanthwal, M., Chauhan,B. S. and Singh,M., "Cationdistribution in mixed Mg-Mn ferrites from X-Ray diffractiontechnique and saturation magnetization", Ind. J. Pure &Appl.Phys., Vol. 44(12), pp. 930-934 (2006).
43. Zaki, H. M., Al-Heniti, S. H., Elmosalami, T. A., "Structural.magnetic and dielectric studies of copper substituted nano-crystalline spinel magnesium zinc ferrite", J. of Alloys and comp.,Vol. 633, pp.104-114 (2015).
44. Caizer, C. Optimization Study on Specific Loss Power in Superparamagnetic Hyperthermia with Magnetite Nanoparticles for High Efficiency in Alternative Cancer Therapy. Nanomaterials 2021, 11, 40. [CrossRef] 32.
45. Caizer, C. Theoretical Study on Specific Loss Power and Heating Temperature in $CoFe_2O_4$ Nanoparticles as Possible Candidate for Alternative Cancer Therapy by Superparamagnetic Hyperthemia. Appl. Sci. 2021, 11, 5505. [CrossRef]